encit 2020

ABCM
Associação Brasileira de Engenharia e Ciências Mecânicas

18th Brazilian Congress of Thermal Sciences and Engineering
November 16–20, 2020 (Online)

ENC-2020-0718
REAL-TIME ESTIMATION OF A POSITION AND TIME DEPENDENT HIGH MAGNITUDE HEAT FLUX IN A 3D NONLINEAR HEAT CONDUCTION PROBLEM BY UNSCENTED KALMAN FILTER

Vítor Fernandes Egger
Mechanical Engineering Department, Universidade Federal Fluminense, TEM/UFF, Niterói, RJ, Brazil
vitoregger@id.uff.br

César Cunha Pacheco
Mechanical Engineering Department, Universidade Federal Fluminense, PGMEC/UFF, Niterói, RJ, Brazil
cesarp@id.uff.br

Abstract. *This paper shows the results obtained in the estimation of a position and time dependent high magnitude heat flux by Unscented Kalman Filter in a three-dimensional nonlinear heat conduction problem. The heat flux is applied to the top surface of a thin flat plate and the heat flux is estimated by using transient temperature measurements taken at the opposite side. The nonlinear behavior of the physical problem is caused by the material properties, which depend on the local temperature. This paper addresses the high computational cost of using a three-dimensional model by using techniques, such as parallelism, algorithm optimization and reduction of dimensionality, to enhance the performance of the Unscented Kalman filter for this physical problem. The obtained values are agreeable and coherent to the referenced values while keeping execution times smaller than simulation times, showing real time execution.*

Keywords: *Unscented Kalman Filter, Heat Conduction, Inverse Problems, Real Time Estimation*

1. INTRODUCTION

Frequently, inverse heat conduction problems involve the estimation of unknown thermal boundary conditions of a heat conduction model through its partially measurable temperature information. Throughout the literature, the application of such class of problems has been analyzed over various engineering and technical fields, such as aerospace, armament, computer, metallurgical and power engineering, as well as nondestructive testing (Pacheco *et al.*, 2015a; Wen *et al.*, 2019; Wan *et al.*, 2020).

During the last few years, sustained research has been aimed at reconstructing a position- and time-dependent high magnitude heat flux. For instance, Orlande *et al.* (2013) utilized a Markov chain Monte Carlo method (MCMC) with a reduced model to estimate the spacially varying high magnitude heat flux. In addition, Pacheco *et al.* (2014a,b, 2015a) researched the uses of Kalman filtering (KF) and its combination with the Improved Lumped Analysis and the Approximate error model for solving the same physical problem while reducing its computational effort. All these approaches utilize a reduced model of the original three-dimensional nonlinear model. For this reason, Pacheco *et al.* (2015b) performed the estimation of a position- and time-dependent high magnitude heat flux in a three-dimensional nonlinear heat conduction problem by utilizing the Unscented Kalman Filter (UKF), a technique from the family of Kalman Filters modified for nonlinear problems (Julier and Uhlmann, 1997) while reporting a very large computational time. Pacheco *et al.* (2016) solved the inverse problem in real-time when resorting to reduced models by utilizing the Steady-State Kalman Filter (SSKF). Similar papers that address this problem using different techniques can be found in the literature, such as Laplace's Transform (Feng *et al.*, 2011), LSQR (Dennis and Dulikravich, 2012) and DCT/Laplace Method (Afrin *et al.*, 2013).

Being inspired by said authors, this work searches to reproduce the results obtained by Pacheco *et al.* (2015b) while incorporating optimizations and analysis for the mathematical and computational models to reduce the computational time. The physical problem considered in this work is the estimation of the heat flux of a three-dimensional nonlinear heat conduction problem and it is solved by UKF. The development is divided in the forward problem and the inverse problem as the forward problem is needed for the UKF. Due to its three-dimensional and nonlinear characteristics, this problem poses a difficult challenge for researchers in the area of inverse problems, having been a subject of several past investigations in the literature (Orlande *et al.*, 2013; Pacheco *et al.*, 2014a,b, 2015a,b). Said authors agree on the difficulty in estimating the heat flux at real time, reporting computational times whose order ranges from minutes to hours, for a situation considering two seconds of physical time. Pacheco *et al.* (2016) reported that real-time estimation

could be achieved by using reduced order modelling and the Steady-State Kalman Filter (Simon, 2006). However, due to linearizations performed in the reduced order modelling, accuracy was lost at the final part of the numerical experiment. Therefore, one concludes that a real-time solution is yet to be achieved.

2. FORWARD PROBLEM

The proposed problem in this paper involves the heating of the top surface of a flat plate as illustrated by Fig. 1. The plate is supposed to be initially at a constant temperature and the heat flux has high magnitude and it is applied in small areas of the top surface. As a result of the high magnitude, temperature dependence of thermophysical properties needs to be taken into account. Heat transfers through the remaining surfaces are considered to be null. In Fig. 1, a, b and c represent the length, the width and the thickness of the plate, respectively.

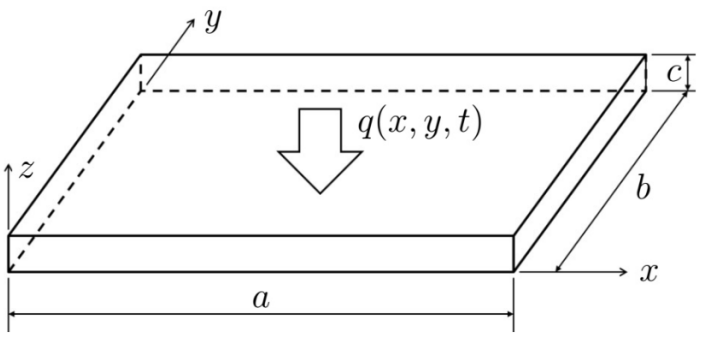

Figure 1: The geometry of the physical problem.

The mathematical model used for the physical problem is the heat conduction equation (Ozisik, 1993) where T represents the temperature and q represents the heat flux in the top surface.

$$C\left(T\right)\frac{\partial T}{\partial t}=\frac{\partial}{\partial x}\left[K\left(T\right)\frac{\partial T}{\partial x}\right]+\frac{\partial}{\partial y}\left[K\left(T\right)\frac{\partial T}{\partial y}\right]+\frac{\partial}{\partial z}\left[K\left(T\right)\frac{\partial T}{\partial z}\right],\quad \text{in}\ \begin{array}{ll}0<x<a, & 0<y<b\\ 0<z<c, & t>0\end{array} \tag{1a}$$

$$\frac{\partial T}{\partial x}=0,\quad \text{at } x=0 \text{ and } x=a,\quad 0<y<b,\quad 0<z<c,\quad t>0 \tag{1b}$$

$$\frac{\partial T}{\partial y}=0,\quad \text{at } y=0 \text{ and } y=b,\quad 0<x<a,\quad 0<z<c,\quad t>0 \tag{1c}$$

$$\frac{\partial T}{\partial z}=0,\quad \text{at } z=0,\quad 0<x<a,\quad 0<y<b,\quad t>0 \tag{1d}$$

$$K\left(T\right)\frac{\partial T}{\partial z}=q\left(x,y,t\right),\quad \text{at } z=c,\quad 0<x<a,\quad 0<y<b,\quad t>0 \tag{1e}$$

$$T=T_0,\quad \text{at } t=0,\quad 0<x<a,\quad 0<y<b,\quad 0<z<c \tag{1f}$$

The temperature-dependent thermal properties C, volumetric heat capacity, and K, thermal conductivity, are given by Eq. (2a)-(2b) (Orlande *et al.*, 2013).

$$C(T)=1324.75T+3557900\quad [\text{J/m}^3\ \text{K}] \tag{2a}$$

$$K(T)=12.45+0.014T+2.517\times10^{-6}T^2\quad [\text{W/mK}] \tag{2b}$$

This three-dimensional nonlinear heat conduction problem was discretized in the space domain by the Finite Volume Method (FVM) (Versteeg and Malalasekera, 2007), which allows the transformation of the partial differential equation into a system of ordinary differential equations represented by Eq. (3), and then solved by using the 4$^{\text{th}}$ Runge-Kutta as initialization and the four-step Adams predictor-corrector pair (Ascher and Greif, 2011). In Eq. (3), **P** represents the boundary heat flux values and **T** represents the vector of temperatures.

$$\frac{\partial \mathbf{T}}{\partial t}=\mathbf{A}(\mathbf{T},C,K,\mathbf{P})\mathbf{T}+\mathbf{b}(\mathbf{P}) \tag{3}$$

3. INVERSE PROBLEM

The inverse problem of estimating the heat flux at the top surface of the plate can be considered as a state estimation problem within the Bayesian framework (Kaipio and Somersalo, 2004). The problem is recast in the form of the evolution-observation model (Simon, 2006; Orlande *et al.*, 2008) given by Eqs. (4a)-(4b). The state vector $\mathbf{x}_k$ contains

the temperature values of all elements in the FVM mesh as well as the discretized heat flux values applied at the top of the control volumes at the $z = c$ surface and the observation vector $\mathbf{y}_k$ is comprised of the temperature values at the $z = 0$ surface. The vector $\mathbf{u}_k$ represents known control functions acting over the dynamic model and is herein assumed to be null. The vectors $\mathbf{v}_k$ and $\mathbf{w}_k$ represent the observation model noise vector that is associated with the covariance matrix $\mathbf{R}_k$ and the evolution model noise vector that is associated with the covariance matrix $\mathbf{Q}_k$, respectively, and they are considered to be Gaussian white noise. The function $\mathbf{f}_k$ represents evolution function while $\mathbf{h}_k$ represents the observation function.

$$\mathbf{x}_{k+1} = \mathbf{f}_k(\mathbf{x}_k, \mathbf{u}_k, \mathbf{w}_k) \tag{4a}$$

$$\mathbf{y}_k = \mathbf{h}_k(\mathbf{x}_k, \mathbf{v}_k) \tag{4b}$$

The complete three-dimensional nonlinear state estimation problem is tackled directly by using the Unscented Kalman Filter (Julier and Uhlmann, 1997; Julier *et al.*, 2000; Wan and R. Van Der Merwe, 2000; Simon, 2006; Pacheco *et al.*, 2015b). The UKF differs from typical algorithms such as the Extended Kalman Filter (EKF) by the manner on how the statistics of the state variables are propagated in time. In the UKF, these propagations process are handled through the Unscented Transformation (Julier *et al.*, 2000), which uses a set of appropriately chosen weight points in order to approximate the mean and covariance of the transformed state. This approach can be referred as an intelligent particle filter (Simon, 2006) since its sampling process occurs in a deterministic and systematic way, differing from the usual random approach of the traditional particle filter algorithms. These selected points are often called sigma points and there are many ways of choosing these points, this work selects its points according to Eq. (5). The notation $[.]_i$ is utilized to get the i^{th} column and the notation $[.]_{i=a:b}$ is used to iterate from the a^{th} column to the b^{th} column, effectively returning a matrix.

$$\mathbf{x}_S = \left[\mathbf{x}; \left[\mathbf{x} + \left[\sqrt{(L+\lambda)\,\mathbf{P}}\right]_i\right]_{i=1:L}; \left[\mathbf{x} - \left[\sqrt{(L+\lambda)\,\mathbf{P}}\right]_i\right]_{i=1:L}\right] \tag{5}$$

The algorithm of the general UKF is presented by Eq. (6a)-(6j), in which $\mathbf{P}$, ${}^{y}_{y}\mathbf{P}$, ${}^{x}_{y}\mathbf{P}$, $\mathbf{Q}$, $\mathbf{R}$ and $\mathbf{K}$ represents the covariance matrix of the state vector, the covariance matrix of the observation vector, the cross covariance matrix between the state vector and the observation vector, the covariance matrix associated with the evolution model noise, the covariance matrix associated with the observation model noise and the Kalman gain, respectively.

$$\mathbf{x}_{S;k+1|k} = \left[\mathbf{f}_k\left(\left[\mathbf{x}_{S;k|k}\right]_i\right)\right]_{i=0:2L} \tag{6a}$$

$$\mathbf{x}_{k+1|k} = \sum_{i=0}^{2L} \mathbf{W}_i^{(m)} \left[\mathbf{x}_{S;k+1|k}\right]_i \tag{6b}$$

$$\mathbf{P}_{k+1|k} = \sum_{i=0}^{2L} \mathbf{W}_i^{(c)} \left(\left[\mathbf{x}_{S;k+1|k}\right]_i - \mathbf{x}_{k+1|k}\right)\left(\left[\mathbf{x}_{S;k+1|k}\right]_i - \mathbf{x}_{k+1|k}\right)^T + \mathbf{Q}_k \tag{6c}$$

$$\mathbf{y}_{S;k+1|k} = \left[\mathbf{h}_k\left(\left[\mathbf{x}_{S;k+1|k}\right]_i\right)\right]_{i=0:2L} \tag{6d}$$

$$\mathbf{y}_{k+1|k} = \sum_{i=0}^{2L} \mathbf{W}_i^{(m)} \left[\mathbf{y}_{S;k+1|k}\right]_i \tag{6e}$$

$${}^{y}_{y}\mathbf{P}_{k+1|k} = \sum_{i=0}^{2L} \mathbf{W}_i^{(c)} \left(\left[\mathbf{y}_{S;k+1|k}\right]_i - \mathbf{y}_{k+1|k}\right)\left(\left[\mathbf{y}_{S;k+1|k}\right]_i - \mathbf{y}_{k+1|k}\right)^T + \mathbf{R}_k \tag{6f}$$

$${}^{x}_{y}\mathbf{P}_{k+1|k} = \sum_{i=0}^{2L} \mathbf{W}_i^{(c)} \left(\left[\mathbf{x}_{S;k+1|k}\right]_i - \mathbf{x}_{k+1|k}\right)\left(\left[\mathbf{y}_{S;k+1|k}\right]_i - \mathbf{y}_{k+1|k}\right)^T \tag{6g}$$

$$\mathbf{K}_{k+1} = {}^{x}_{y}\mathbf{P}_{k+1|k}\left({}^{y}_{y}\mathbf{P}_{k+1|k}\right)^{-1} \tag{6h}$$

$$\mathbf{x}_{k+1|k+1} = \mathbf{x}_{k+1|k} + \mathbf{K}_{k+1}\left(\mathbf{y}_{k+1} - \mathbf{y}_{k+1|k}\right) \tag{6i}$$

$$\mathbf{P}_{k+1|k+1} = \mathbf{P}_{k+1|k} - \mathbf{K}_{k+1}\,{}^{y}_{y}\mathbf{P}_{k+1|k}\left(\mathbf{K}_{k+1}\right)^T \tag{6j}$$

The sigma points are composed of a set of length $2L+1$, where L is the dimensionality of the state vector $\mathbf{x}$. The zeroth sigma point is equal to the posterior estimate of the previous time step $\mathbf{x}_{k|k}$ and the other $2L$ sigma points are obtained by adding or subtracting each column of $\sqrt{(L+\lambda)\mathbf{P}_{k|k}}$ to $\mathbf{x}_{k|k}$ (Pacheco *et al.*, 2015b). The parameter $\lambda = \alpha^2\,(L+\kappa) - L$ represents a scaling factor. The parameters α, β and κ represents the spread of the sigma points, the knowledge of the

previous distribution and a secondary scaling factor, respectively. Usually, these parameters are set to be equal to 10^{-3}, 2 and 0 (Wan and R. Van Der Merwe, 2000), respectively. There is a weight that is represented by $\mathbf{W}$ associated to each sigma point for the estimation of the new mean and covariance described by Eq. (7a)-(7c), where the superscript "m" and "c" refers to the mean and covariance, respectively.

$$\mathbf{W}_0^{(m)} = \frac{\lambda}{L+\lambda} \tag{7a}$$

$$\mathbf{W}_0^{(c)} = \frac{\lambda}{L+\lambda} + \left(1 - \alpha^2 + \beta\right) \tag{7b}$$

$$\mathbf{W}_i^{(m)} = \mathbf{W}_i^{(c)} = \frac{1}{\lambda\left(L+\lambda\right)} \text{ for } i = 1, \ldots, 2L \tag{7c}$$

The evolution of the temperature values is calculated by solving the forward problem for one time step with the values of heat flux maintained as constant. The observation function consists in taking the state vector as input and the values of temperature of the bottom surface as outputs.

This mathematical model can be optimized in the steps described by Eq. (6c)-(6g) due to the observation function only selecting values from the state vector. In other words, the calculation of the empirical mean and covariance matrix of the transformed points and the cross-covariance matrix can be reduced to a slice of the a priori estimate of the state vector and of the calculated sum of covariances of each sigma point. Equations (8a)-(8e) describe this optimization. The $Slice$ operator receives as input a vector and an one-dimensional size or a matrix and a two-dimensional size and returns a new vector or matrix with the firsts elements up to the size of the input vector or matrix, respectively. The $Size$ operator receives a vector or a matrix and returns the number of elements that it contains in an one-dimensional size or a two-dimensional size, respectively.

$$\mathbf{P}_{h;k+1|k} = \sum_{i=0}^{2L} \mathbf{W}_i^{(c)} \left(\left[\mathbf{x}_{S;k+1|k}\right]_i - \mathbf{x}_{k+1|k}\right)\left(\left[\mathbf{x}_{S;k+1|k}\right]_i - \mathbf{x}_{k+1|k}\right)^T \tag{8a}$$

$$\mathbf{P}_{k+1|k} = \mathbf{P}_{h;k+1|k} + \mathbf{Q}_k \tag{8b}$$

$$\mathbf{y}_{k+1|k} = Slice\left(\mathbf{x}_{k+1|k}, Size\left(\mathbf{y}_{k+1|k}\right)\right) \tag{8c}$$

$${}_y^y\mathbf{P}_{k+1|k} = Slice\left(\mathbf{P}_{h;k+1|k}, Size\left({}_y^y\mathbf{P}_{k+1|k}\right)\right) + \mathbf{R}_k \tag{8d}$$

$${}_y^x\mathbf{P}_{k+1|k} = Slice\left(\mathbf{P}_{h;k+1|k}, Size\left({}_y^x\mathbf{P}_{k+1|k}\right)\right)) \tag{8e}$$

To talk about computational costs and runtimes, it is necessary to introduce the asymptotic notation. The O-notation, the Ω-notation and the Θ-notation is used to represent an asymptotic upper bound, lower bound and tight bound, respectively (Cormen *et al.*, 2009). While this algorithm is bounded by the orders $O(L_t L^3)$ and $\Omega(L_t L^2)$ where L_t is the number of temporal subdivision, the implementation can vary wildly. Furthermore, while the reduction of the computational cost order is desirable, recent technologies made the parallel approach with higher order faster than lower order implementations for an adequate dimensionality. The bottlenecks for this algorithm are the high-order methods such as Cholesky decompositions, the sum of covariance matrices and the matrix inversion. While each of them have independent parallel aproaches, the speed gain is normally at the order of the dimensionality. On the other hand, the calculation of the forward problem in the evolution step is not considered a bottleneck despite the possibility of higher order costs because it is $\Theta(L)$ in the simplest approach using Euler's method.

Considerations are made to speed up the calculation such as using parallelism, a more powerful computer and, if it is not enough, reduction of the dimensionality. The parallelism is tackled in the mathematical approach while the last two are considered after analyzing the performance of the main algorithm. Thus, all code was properly built for GPU usage utilizing CUDA technology, where parallelism is native (NVIDIA, 2020a). The biggest bottlenecks mentioned are solved by using dedicated libraries created by NVIDIA, especially CuBLAS and CuSolver (NVIDIA, 2020b). The new operator $Slice$ is a memory copy of the input vector inside the GPU memory. Furthermore, the memory copy is faster than the summation of vectors or matrices needed in the original algorithm. The combination of the parallel implementation and the optimized algorithm is called Optimized Parallel Algorithm (OPA).

4. RESULTS AND DISCUSSIONS

In order to test the viability of the proposed approach, a numerical experiment was performed, considering a set of synthetic measurements generated as follows. The forward problem was solved using a temperature grid of sizes $59 \times 59 \times 13$ with 4096 time steps within 2 s of physical time. The dimensions of the plate are assumed to be 120, 120 and 3 mm. The heat flux applied at the top surface is defined by Eq. (9). The standard deviation σ_{Tm} associated with

measurement errors is assumed to be equal to 1.25 K. Figure 2a represents the evolution of temperature at center point of the bottom surface, while Fig. 2b represents the temperature profile of the bottom surface at $t = 2s$.

$$q\left(x,y,t\right) = \begin{cases} 5\times10^{6}, & \text{if } 48 \text{ mm} \leq x \leq 84 \text{ mm and } 48 \text{ mm} \leq y \leq 84 \text{ mm} \\ 0, & \text{otherwise} \end{cases} \quad \left[\text{W/m}^2\right] \tag{9}$$

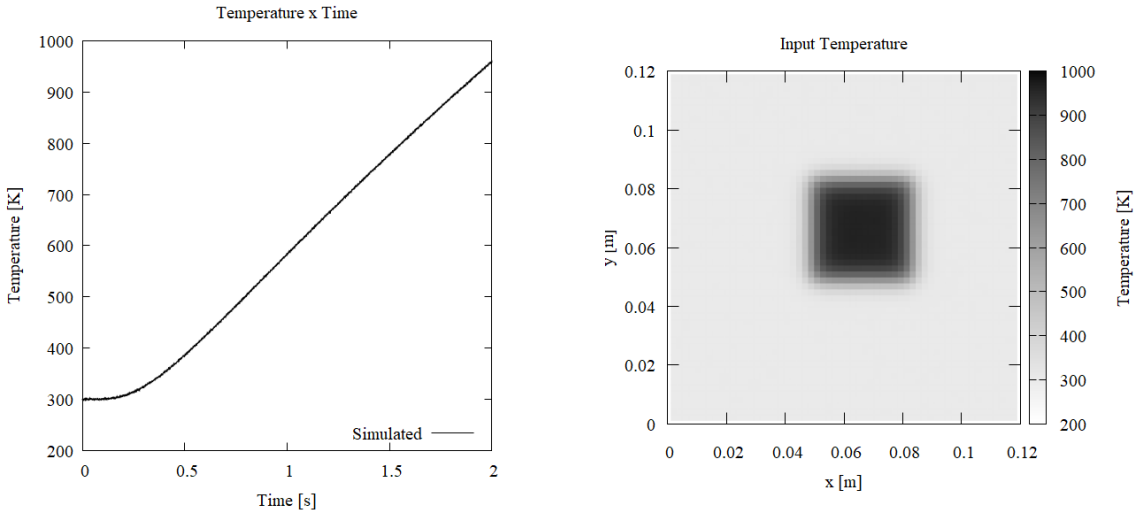

(a) (b)

Figure 2: Generation of synthetic temperature measurements: (a) time evolution at the center of the $z = 0$ surface; and (b) Contour lines at the $z = 0$ surface at $t = 2$ s

The input data is considered acceptable as the temperature curve is increasing with the inwards heat flux. Furthermore, these values are supposed to be close enough to be interpolated trilinear in the spatial axis, x and y and time axis to the same grid size as the input for the inverse problem.

The inverse problem was solved in a $24 \times 24 \times 6$ computational grid, resulting in 3456 values of temperature and 576 values of heat flux, adding up to a total of 4032 state variables, which is the dimensionality of the state vector. The temporal subdivision L_t is chosen to be equal to 100, leading to a time step of 0.02 s. The synthetic measurements are assumed available at each time step for every control volume at the $z = 0$ surface. The estimated values of temperature at the bottom surface of the plate at $t = 2$ s are shown in Fig. 3a and the estimated heat flux values at the top surface are shown in Fig. 3b. One can observe that an excellent agreement was achieved between estimated and reference values.

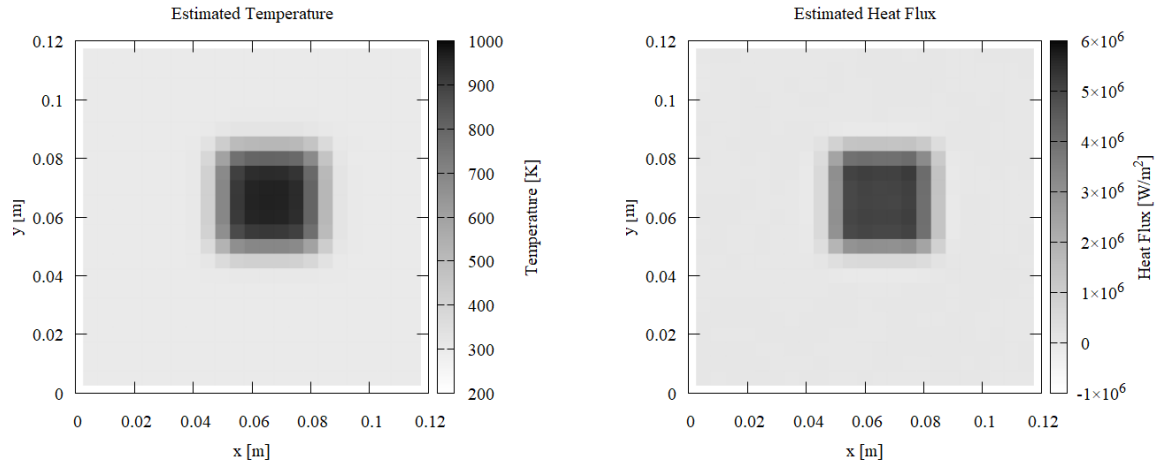

(a) (b)

Figure 3: Results obtained with the UKF at $t = 2$ s: (a) estimated temperature at the bottom surface; and (b) estimated heat flux at the top surface.

The time evolution of the estimated and synthetic values is also analyzed. It was selected the center of the xy plane to represent the temperature and heat flux evolution as it is close to the center of the heating. Figures 4a and 4b show the temperature and heat flux evolution, respectively.

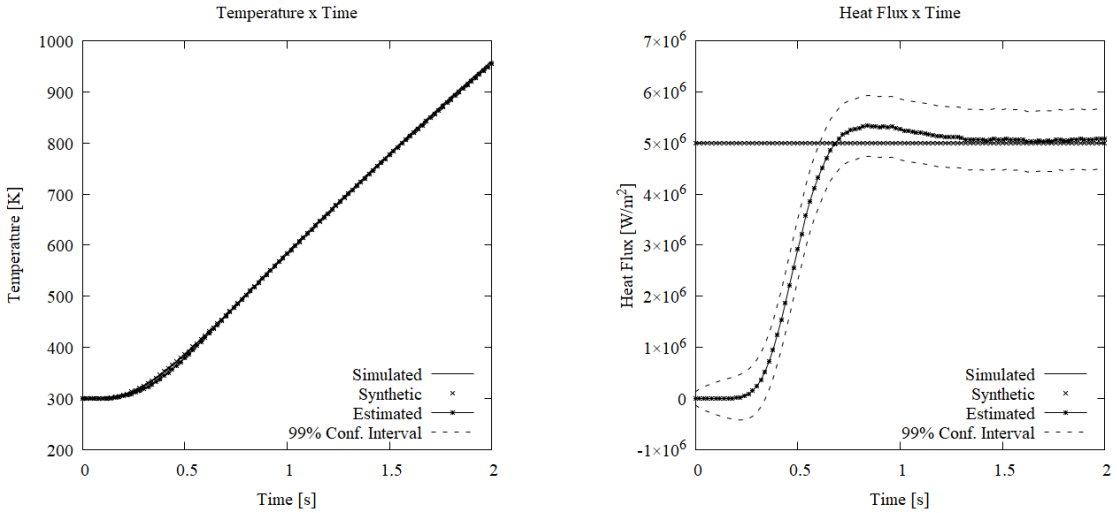

(a) (b)

Figure 4: Time evolution of estimated and synthetic values: (a) temperature at the center of the bottom surface; and (b) heat flux at the center of the top surface.

The evolution of temperature residuals is shown in Fig. 5a to quantify how much the estimated temperature values differ from the synthetic ones. The residuals peak around $t = 0.46$ s, caused by the delay needed for the temperatures at the opposite side of the plate to exceed the measurement error values. For the remainder of the numerical experiment, the residuals show no correlation, oscillating around zero with amplitude of the same order of magnitude of σ_{T_m}. The contour lines of the residuals at $t = 0.46$ s which are presented in Fig. 5b show that the residuals are concentrated only in the heating surface.

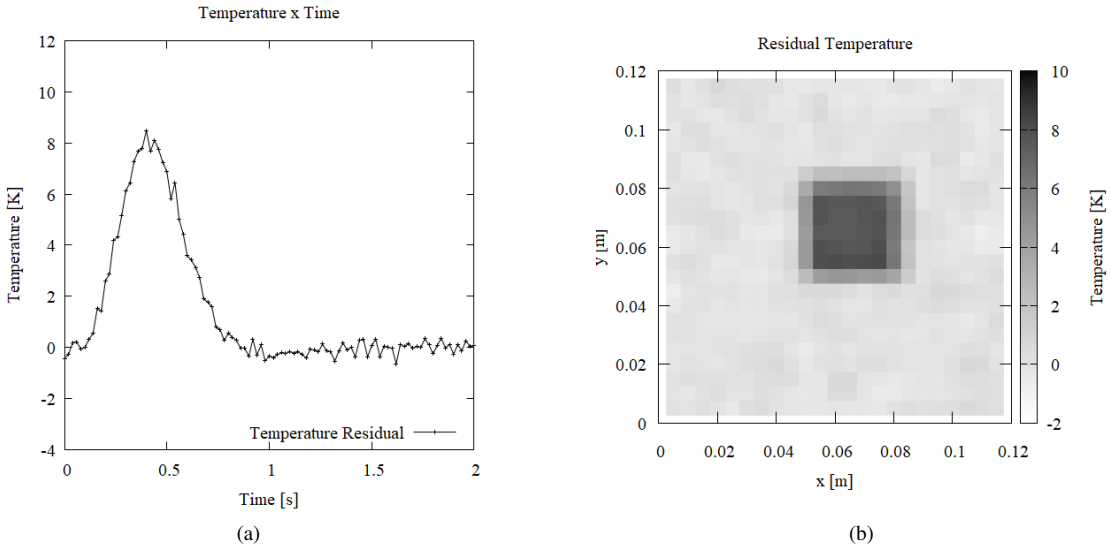

(a) (b)

Figure 5: Analysis of the residuals: (a) values at the center of the bottom surface; and (b) values at the bottom surface at $t = 0.46$ s.

Despite having considerable agreement between the estimated data and the synthetic data, the execution time is still on the order of minutes. While this is an improvement compared to previous works (Orlande *et al.*, 2013; Pacheco *et al.*, 2014a, 2015a,b, 2016), there are still improvements that can be made, such as the reduction of the dimensionality and the utilization of powerful hardware.

The reduction of the dimensionality of the inverse problem results in a lower grid size, in a lower temporal subdivision, but also in a lower precision. Furthermore, it is paramount to abide the stability conditions of the solution of the forward problem. To perform this reduction, it was considered lowering the temporal subdivision L_t, the x and y axis subdivisions representing the surface subdivision L_s and the z axis subdivision L_z. The surface subdivision is equal to the subdivision of the x axis and the y axis. The order of the UKF algorithm implies in a linear reduction by reducing L_t and a superlinear

reduction by reducing L_s or L_z being, at least, quadratically in the dimensionality of the state vector and it can be seen in Fig. 6a, Fig. 7a and Fig. 8a. The loss in precision is acceptable, specially when considering that the 99% confidence interval of the estimated heat flux encapsulates the exact value after stabilizing.

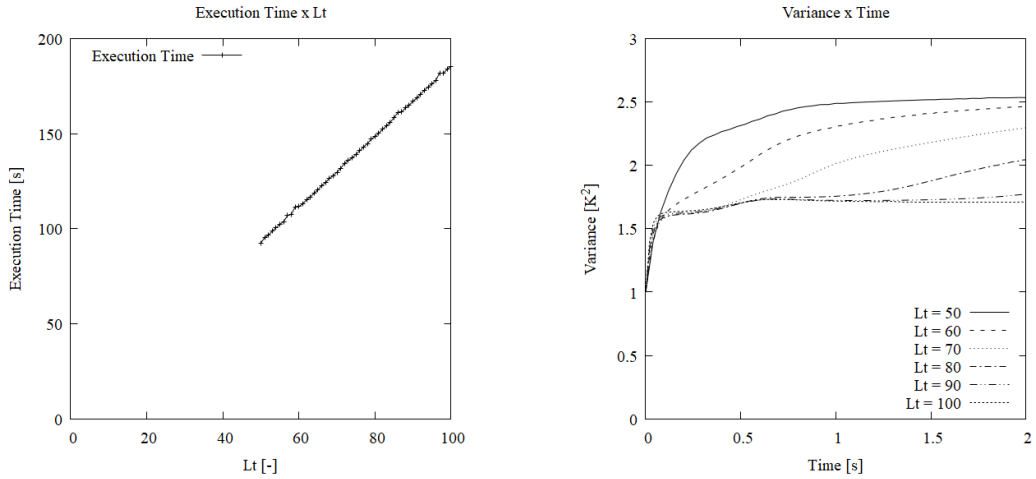

(a) (b)

Figure 6: Analysis of reductions of L_t: (a) execution time; and (b) evolution of the temperature variance at the center of the bottom surface.

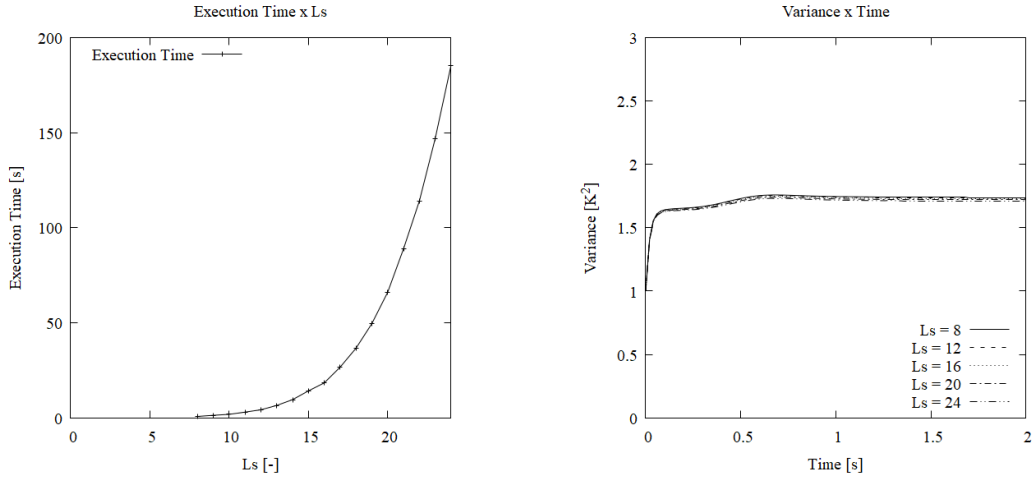

(a) (b)

Figure 7: Analysis of reductions of L_s: (a) execution time; and (b) evolution of the temperature variance at the center of the bottom surface.

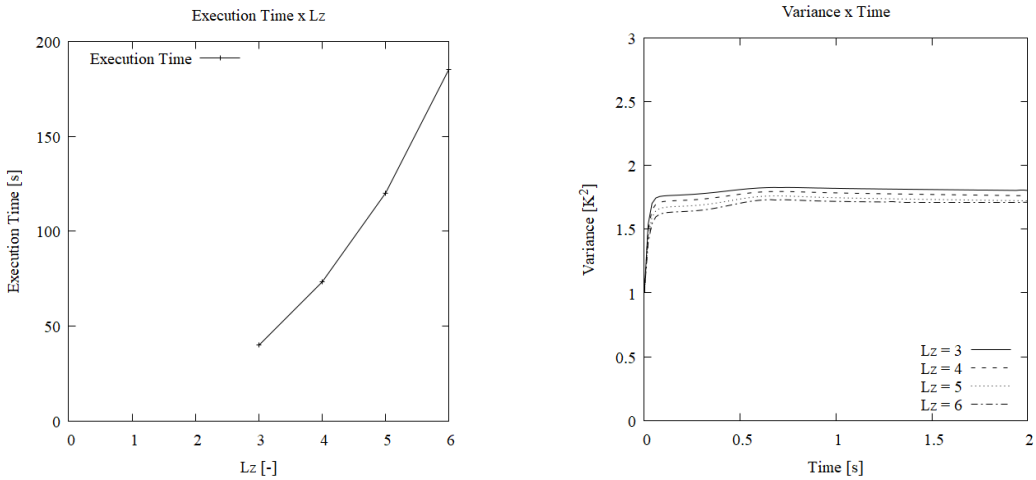

(a) (b)

Figure 8: Analysis of reductions of L_z: (a) execution time; and (b) evolution of the temperature variance at the center of the bottom surface.

The reduced dimensions for a case comparison was chosen to be $L_t = 50$, $L_x = L_y = 12$ and $L_z = 6$ and the results are described by Fig. 9a and Fig. 9b. While the algorithm with a coarse grid converges to the synthetic values, the synthetic values for the coarse grid are not as close to the simulated values as the fine grid implying in a second loss of precision by trying to use a trilinear interpolation.

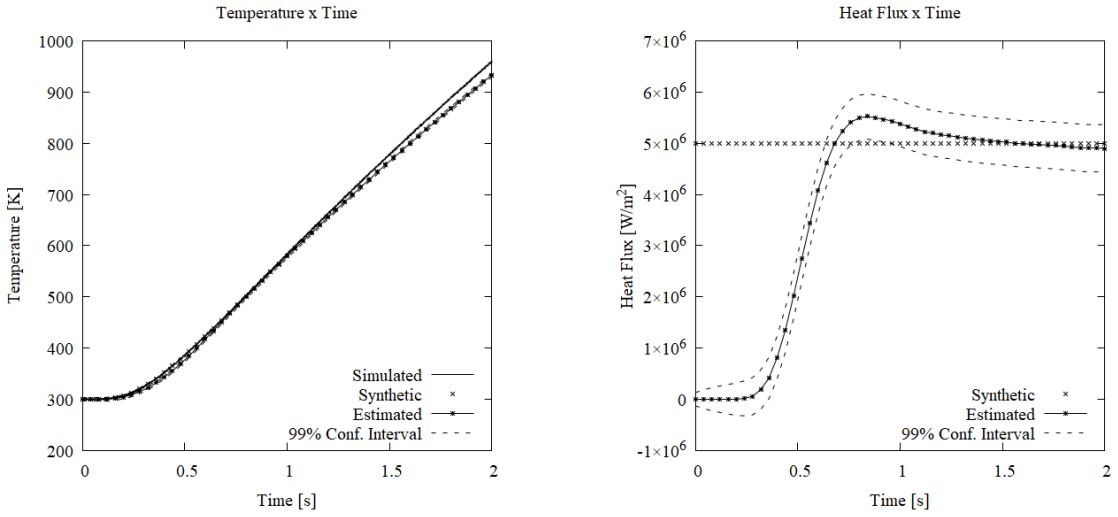

(a) (b)

Figure 9: Time evolution of the results in a $12 \times 12 \times 6$ grid with 50 time steps: (a) temperature at the bottom surface; (b) heat flux at the top surface.

While reaching real time calculations with certain reductions, it is still possible to use powerful computers to gain improvements. It was utilized a workstation to solve the inverse problem with no reduction and with a chosen reduction of $12 \times 12 \times 6$ with 50 temporal steps, obtaining the execution times of $10.306s$ and $0.37819s$, respectively. The result of the execution time of the reduced grid is considered real time calculation due to being smaller than and not close to the simulation time. Table 1 shows each execution time for all the improvements made and also for previous publications on this problem. It is possible to observe that the present approach was not only successful in solving the inverse problem in real time, but not requiring use of reduced models, as was done in previous works.

Table 1: Computational times for the numerical experiments.

Author	Reduced Modelling	Method	Time
(Orlande *et al.*, 2013)	Y	MCMC	2.7 h
(Pacheco *et al.*, 2015a)	Y	KF	5 min
(Pacheco *et al.*, 2015b)	N	UKF	32 h
(Pacheco *et al.*, 2016)	Y	SSKF	0.9 s
Present Work – Serial	N	UKF	16 h
Present Work – OPA	N	UKF	185.45 s
Present Work – OPA + Server	N	UKF	10.31 s
Present Work – OPA + Reduced Grid	N	UKF	2.14 s
Present Work – OPA + Server + Reduced Grid	N	UKF	0.37 s

5. CONCLUSION

In this work, the algorithm UKF was optimized using a few techniques to solve and to reach real time calculation for the estimation of the heat flux in a three-dimensional nonlinear heat conduction problem. Although only one set of data was utilized, there were no optimization specifically for this data, proving real time possibility for this problem using UKF and no reduced model. Still, this inverse problem has an undesirable computational order, resulting in unfeasibility of this model if the grid sizes are increased in every direction.

For future researches, there are three lines of thought to further improve on this problem. The first one is to validate this work with actual experimental data and, if possible, test this approach as a virtual sensor. The second one is to utilize other and newer technologies or hardware to further enhance the performance, a few examples that may improve performance is to better organize the working threads to reduce the number of synchronization points, change the memory layout to improve data access speeds or to just use better and faster hardware. While the final one is to explore new mathematical optimizations or methods to achieve lower computational orders, a few examples are the utilization of the sparsity or

locality of the problem to reduce the number of needed calculations, the discovery of new mathematical optimizations or properties to enhance efficiency or even the change of main algorithm that solves the inverse problem.

6. REFERENCES

Afrin, N., Feng, Z.C., Zhang, Y. and Chen, J.K., 2013. "Inverse Estimation of Front Surface Temperature of a Locally Heated Plate with Temperature-dependent Conductivity via Kirchhoff Transformation". *Int. J. Therm. Sci.*, Vol. 69, pp. 53–60.

Ascher, U.M. and Greif, C., 2011. *A First Course in Numerical Methods*. Society for Industrial and Applied Mathematics. ISBN 0-89871-997-6.

Cormen, T.H., Leiserson, C.E., Rivest, R.L. and Stein, C., 2009. *Introduction to Algorithms, Third Edition*. The MIT Press, 3rd edition. ISBN 0262033844.

Dennis, B.H. and Dulikravich, G.S., 2012. "Inverse Determination of Unsteady Temperatures and Heat Fluxes on Inaccessible Boundaries". *Inverse Ill-Posed Probl.*, Vol. 20, No. 5–6, pp. 791–803.

Feng, Z.C., Chen, J.K., Zhang, Y. and Griggs Jr., J.L., 2011. "Estimation of Front Surface Temperature and Heat Flux of a Locally Heated Plate from Distributed Sensor Data on the Back Surface". *Int. J. Heat Mass Transf.*, Vol. 54, pp. 3431–3439.

Julier, S., Uhlmann, J. and Durrant-Whyte, H.F., 2000. "A new method for the nonlinear transformation of means and covariances in filters and estimators". *IEEE Transactions on Automatic Control*, Vol. 45, No. 3, pp. 477–482. ISSN 1558-2523. doi:10.1109/9.847726.

Julier, S.J. and Uhlmann, J.K., 1997. "New extension of the Kalman filter to nonlinear systems". In *Proc.SPIE*. Vol. 3068. doi:10.1117/12.280797.

Kaipio, J.P. and Somersalo, E., 2004. *Statistical and Computational Inverse Problems*. Springer Science+Business Media, Inc. ISBN 978-0-387-22073-4.

NVIDIA, 2020a. "Cuda c++ programming guide". `https://docs.nvidia.com/cuda/pdf/CUDA_C_Programming_Guide.pdf`. Accessed: 2020-07-17.

NVIDIA, 2020b. "Cuda toolkit documentation - v11.0.194". `https://docs.nvidia.com/cuda/index.html`. Accessed: 2020-07-17.

Orlande, H.R.B., Dulikravich, G.S., Neumayer, M., Watzenig, D. and Colaço, M.J., 2013. "Accelerated Bayesian Inference for the Estimation of Spatially Varying Heat Flux in a Heat Conduction Problem". *Numerical Heat Transfer, Part A: Applications*, Vol. 65, No. 1, pp. 1–25.

Orlande, H.R.B., Dulikravich, G.S. and Colaço, M.J., 2008. "Application of Bayesian Filters to Heat Conduction Problems". In *EngOpt - International Conference on Engineering Optimization*. Rio de Janeiro, Brazil.

Ozisik, M.N., 1993. *Heat Conduction*. John Wiley & Sons, Inc., 2nd edition.

Pacheco, C.C., Orlande, H.R.B., Colaço, M.J. and Dulikravich, G.S., 2016. "Real-time identification of a high-magnitude boundary heat flux on a plate". *Inverse Problems in Science and Engineering*, Vol. 0, No. 0, pp. 1–19. doi:10.1080/17415977.2016.1195829.

Pacheco, C.C., Orlande, H.R.B., Colaço, M.J. and Dulikravich, G.S., 2014a. "Estimation of a Spatial and Time Dependent High Magnitude Heat Flux Using the Kalman Filter". In *15th Brazilian Congress of Thermal Sciences and Engineering*.

Pacheco, C.C., Orlande, H.R.B., Colaço, M.J. and Dulikravich, G.S., 2014b. "Identification of a position and time dependent heat flux using the Kalman filter and improved lumped analysis in heat conduction". In *5th International Conference on Computational Methods*.

Pacheco, C.C., Orlande, H.R.B., Colaço, M.J. and Dulikravich, G.S., 2015a. "Estimation of a location-and-time dependent high magnitude heat flux in a heat conduction problem using the Kalman filter and the approximation error model". *Numerical Heat Transfer, Part A*, Vol. 68, No. 11, pp. 1198–1219.

Pacheco, C.C., Orlande, H.R.B., Colaço, M.J. and Dulikravich, G.S., 2015b. "Identification of a Position and Time Dependent Heat Flux Using the Unscented Kalman Filter in 3D Nonlinear Heat Conduction". In *14th UK Heat Transfer Conference*. Edinburg, UK.

Simon, D., 2006. *Optimal State Estimation: Kalman, H Infinity, and Nonlinear Approaches*. John Wiley & Sons, Inc. ISBN 978-0-471-70858-2.

Versteeg, H.K. and Malalasekera, W., 2007. *An Introduction to Computational Fluid Dynamics: The Finite Volume Method*. Longman Group Ltd, 2nd edition.

Wan, E.A. and R. Van Der Merwe, 2000. "The unscented Kalman filter for nonlinear estimation". In *Proceedings of the IEEE 2000 Adaptive Systems for Signal Processing, Communications, and Control Symposium (Cat. No.00EX373)*. pp. 153–158. doi:10.1109/ASSPCC.2000.882463.

Wan, S., Xu, P., Wang, K., Yang, J. and Li, S., 2020. "Real-time estimation of thermal boundary of unsteady heat conduction system using PID algorithm". *Int. J. Therm. Sci.*, Vol. 153, No. 106395.

Wen, S., Qi, H., Yu, X.Y., Ren, Y.T., Wei, L.Y. and Ruan, L.M., 2019. "Real-time estimation of time-dependent imposed heat flux in graded index media by KF-RLSE algorithm". *Applied Thermal Engineering*, Vol. 150, pp. 1–10.

7. RESPONSIBILITY NOTICE

The authors are solely responsible for the printed material included in this paper.